INSTITUTE OF PHYSICS PUBLISHING JOURNAL OF OPTICS A: PURE AND APPLIED OPTICS
J. Opt. A: Pure Appl. Opt. **6** (2004) S91–S99 PII: S1464-4258(04)67964-5

The influence of depolarization and corneal birefringence on ocular polarization

Juan M Bueno

Laboratorio de Óptica, Universidad de Murcia, Campus de Espinardo (Edificio C), 30071, Murcia, Spain

E-mail: bueno@um.es

Received 22 August 2003, accepted for publication 13 January 2004
Published 24 February 2004
Online at stacks.iop.org/JOptA/6/S91 (DOI: 10.1088/1464-4258/6/3/016)

Abstract
The polarization state of light double passing through the eye is mainly modified by the birefringent structures of the cornea and the retina. The effects of depolarization are often light in normal young eyes but these could change with age, ocular pathologies and refractive surgery. The influence of depolarization on the calculation of the ocular retardation has been studied. Results show that the larger the depolarization, the larger the error in the computed ocular retardation. Moreover, the influence of the corneal compensation on measurements of ocular polarimetry has also been explored. We found that an incomplete compensation of the retardation and/or corneal axis leads to both wrong estimation of the ocular retardation and an erroneous computation of the corneal axis.

Keywords: retardation, depolarization, corneal birefringence, polarimetry, polarization

1. Introduction

Measurement of the changes in the polarization state of light passing through the eye is a very useful tool for investigating ocular media. The eye has complex polarization properties, which arise from both the different internal natures of the ocular elements and their particular spatial arrangement (see [1] as a general reference). These properties are even more relevant when the eyes undergo some kind of surgery or suffer from some pathology.

It is well known that polarization is intrinsically related to the physical properties of an optical medium [2]. On the other hand, ocular surgeries and pathologies may change the physical and mechanical properties of the eye. Then, changes in polarization could be used in clinical diagnosis and post-surgery control.

For almost 200 years, ocular polarization properties have been objects of many diverse studies. However, in the early 1990s, scanning laser polarimetry oriented to the detection of glaucoma [3, 4] was the origin of a very valuable technique in ophthalmologic diagnosis. Polarimetric and histological measurements of *in vitro* retinas were compared to check the reliability of this technique in assessing retinal thickness [5].

However, the study of *in vivo* retinas is much more complicated. A light beam emerging from the living eye after a double pass (DP) through the ocular optics contains information on the polarization properties of all ocular structures (cornea, lens, retina and humours). Humours are optically inactive [1] and the contribution of the lens has been reported to be weak [6–8]. In contrast, the cornea and the retina are clearly birefringent [9–17]. In this sense, the information extracted from the emergent light combines corneal and retinal contributions. In particular, when keeping the point of incidence constant over the corneal surface and scanning the retina, values of the global ocular retardation will be maximum (minimum) where the corneal and retinal fast axes are parallel (perpendicular) [14, 18]. In these conditions the ocular retardation map for the macular area shows a bow-tie pattern centred on the fovea. As a direct consequence, and in terms of retardation, the corneal contribution could lead to an erroneous determination of the retinal information.

To avoid this, the earlier commercial scanning laser polarimeters included a fixed corneal compensator (also called

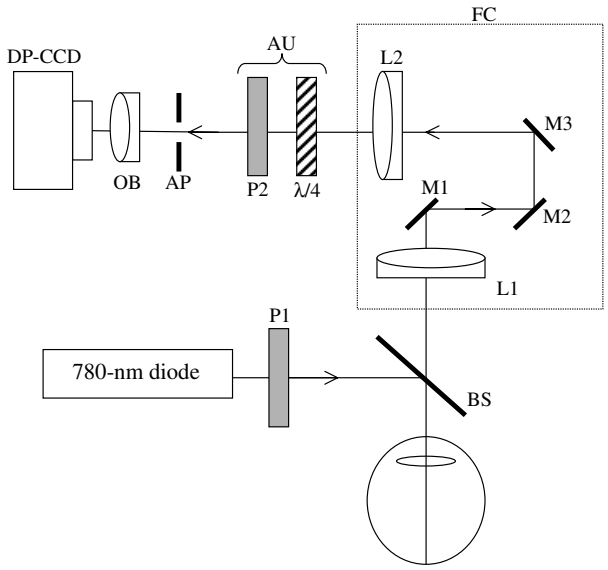

Figure 1. A simplified schematic diagram of the DP imaging polarimeter. M_1–M_3: mirrors; AP: artificial pupil; BS: pellicle beam splitter. Further details are provided in the text.

an anterior segment compensator) consisting of a linear retarder with the fast axis oriented at 15° in the nasally downward (ND) direction and a retardation of 60 nm [19]. However, corneal polarization parameters may vary over a wide range [11, 19] and the impact of a fixed corneal compensation on measurements of retinal thickness could be important [19–21]. These disadvantages have led to the development of a new method for assessment and compensation of both the retardation and the axis of the anterior ocular segment, which has been recently reported to be more accurate and reliable [22–24]. This set-up uses a variable compensator to cancel or minimize the birefringence map at the macular area in each individual eye. A correct corneal compensation provides a uniform brightness and a profile that is flat and equal to the macular DP retardation. Once the maximum compensation is reached (the more uniform the map, the better the compensation), measurements around the optic nerve head (or papilla) are carried out. When total compensation is not reached, the macular retardation map still presents a bow-tie pattern.

All this refers to normal healthy eyes and supposes the central cornea to be a linear retarder. However, older eyes may also have some age-related macular diseases which might change their physical properties. Since commercial polarimeters do not calculate the complete Mueller matrix, the depolarizing effects are not really taken into account and the method may fail because of changes in retinal structure and increase in depolarization processes [25, 26]. Moreover, it has been reported that refractive surgery modifies biomechanical corneal properties [27] and increases the ocular scattering [28], and could also have some influence on retinal polarimetry [29, 30]. In view of this, the present work was proposed to gain understanding of the role of ocular depolarization and corneal birefringence in the accurate assessment of the ocular polarization properties.

2. Methods

To obtain information on living human eyes we have used a modified DP imaging polarimeter [15, 31]. Figure 1 shows a schematic diagram of the experimental system. A collimated infrared laser beam (780 nm wavelength and 1.5 mm in diameter) vertically polarized (by use of P1) enters the eye. After reflection in the retina, the outgoing beam passes through an optometer-based focus corrector system (FC) and propagates through the analyser unit (AU, composed of a rotatory retarder ($\lambda/4$) and a vertical linear polarizer (P2)), and reaches the recording stage (a cooled scientific-grade CCD camera, DP-CCD). The size of the beam is limited to 5 mm by the AP (conjugated with the pupil's eye by means of the achromatic doublets L1 and L2) and an objective (OB) of 50 mm focal length makes it focus on the CCD plane.

During measurements the head of the subject was stabilized with a bite-bar mounted on a three-axis positioning stage. To control the correct positioning of the subject's natural pupil during exposures, an additional video camera (not shown in figure 1) was also used. All the subjects involved in the present study showed no ocular pathology and had a corrected visual acuity of 20/20 or better.

A series of four DP images corresponding to independent polarization states in the AU were recorded (1 s exposure time). The independent polarization states correspond to four orientations of the fast axis of the retarder (−45°, 0°, 30° and 60°) [10]. Once the images were registered, the information on ocular polarization properties was obtained from the Stokes vector associated with the light emerging from the eye, S_{OUT}. This vector can be computed as

$$S_{\mathrm{OUT}} = \begin{pmatrix} S_0 \\ S_1 \\ S_2 \\ S_3 \end{pmatrix} = (M_{\mathrm{PSA}})^{-1} \begin{pmatrix} I_1 \\ I_2 \\ I_3 \\ I_4 \end{pmatrix} \tag{1}$$

where M_{PSA} is the auxiliary matrix defined in [32]. In general the I_i ($i = 1, 2, 3, 4$) are the intensities at each pixel of the four registered images. For the particular purposes of this paper, the I_i are the averaged intensities for a circular area of 2.6 min of arc in diameter centred on the peak of the corresponding DP image.

It has been reported that, apart from some light depolarizing effects [33, 34], linear birefringence is the most relevant polarization property of a healthy eye. In these conditions, the calculation of the complete Mueller matrix is not necessary [35]. Taking into account the expression for the Mueller matrix of a linear retarder in combination with a partial depolarizer [36], the parameters of polarization, such as the degree of polarization (DOP), and the retardation (δ) and the axis (α) related to birefringence can be computed as

$$\begin{aligned} \mathrm{DOP} &= \frac{\sqrt{S_1^2 + S_2^2 + S_3^2}}{S_0} \\ \alpha &= \frac{1}{2} a\tan\left(-\frac{\mathrm{DOP} + S_1}{S_2}\right) \\ \delta &= a\cos\left(1 + \frac{2S_2}{\mathrm{DOP}\sin(4\alpha)}\right). \end{aligned} \tag{2}$$

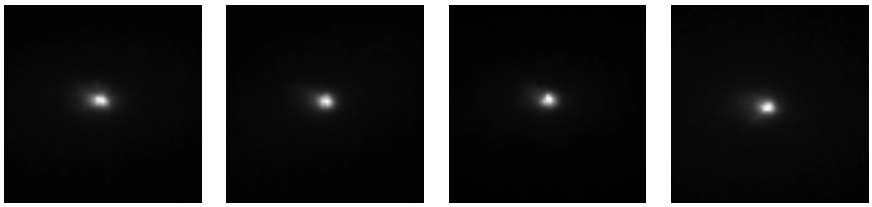

Figure 2. DP images for the same subject corresponding to the four independent polarization states in the AU (−45°, 0°, 30° and 60°). The images subtend 3°.

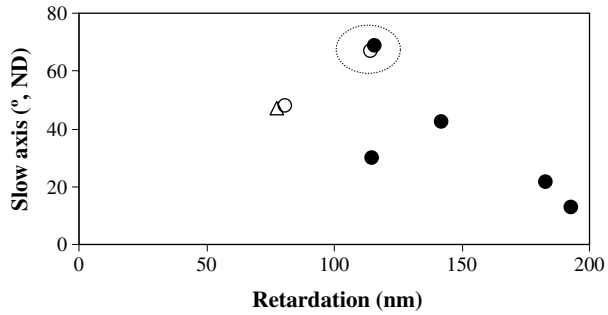

Figure 3. The corneal retardation and slow axis (black symbols) for five adult subjects. Three additional data from [15] are also included for comparison (white symbols). Encircled symbols correspond to the same subject, the measurements being taken with two different polarimeters four years apart (see the text for further details).

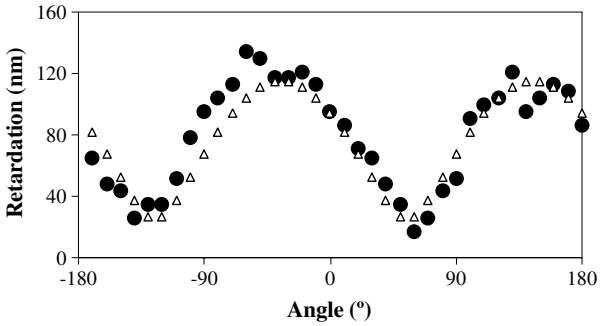

Figure 4. Ocular retardation along a circle around the centre of the fovea for the right eye of a young adult subject (black circles). The origin of the angle (0°) is in the horizontal nasal meridian and values increase in the anticlockwise direction. White triangles represent the fit to the polarization-based model eye proposed in section 3.3.

Throughout this paper the term 'depolarization' will refer to the parameter calculated as 1-DOP.

On the other hand, the results presented in section 3.3 were obtained from two commercial scanning laser polarimeters: the classical GDx Nerve Fiber Analyzer and the GDx VCC (Laser Diagnosis Technologies, Inc., San Diego, CA) with fixed and variable corneal compensators respectively.

3. Results

3.1. Polarization properties of the living human eye

As an example, figure 2 presents the DP images corresponding to the four polarization states produced in the AU for one of the subjects. As explained above, polarimetric calculations were done for the central part of the DP images and the computed polarization parameters are thought to be mainly associated with the corneal birefringence [15, 32].

Figure 3 shows the results on the retardation (for a DP through the eye) and slow axis for five young adult subjects (aged 24–41, two left eyes and three right eyes). Since commercial scanning laser polarimeters show the retardation in nanometres, we have decided to present our results in nm instead of in degrees. This allows direct comparison with earlier reported values. The slow axis has been referred to the ND direction. For the sake of completeness the figure also includes the data reported in [15] (white symbols) measured with a different experimental system.

For this set of subjects, retardation varied from 115 to 193 nm (77–193 when including all the data). The orientations of the corneal axis also depended on the subject, but they were always along the upper temporal to lower nasal direction.

In order to validate the results obtained with our experimental set-up we proceeded as follows. Measurements on one of the subjects (marked with a dashed circle in figure 3) were made under two different sets of experimental conditions. The subject is one of the subjects studied in [15]. Measurements for this observer were carried out four years ago by using a DP liquid-crystal imaging polarimeter and for this work by means of the set-up described above. It can be seen that the results are similar.

Moreover, measurements of the right eye of one of the subjects (corresponding to a white triangle in figure 3) were also made with a confocal scanning laser ophthalmoscope which incorporated a polarimeter (this experimental set-up was described in detail in [37]). For the central part of the fovea the total retardation (in a DP) was 75 nm. The orientation of the slow axis was 40° (ND) for this area, which corroborates the well-known ND direction. The corresponding data obtained from the DP imaging polarimeter were 79 nm for the retardation and 47° ND for the slow axis. The results obtained with the two techniques are comparable and show the reliability of the experimental system developed in our laboratory.

In figure 4 the ocular retardation (for a DP) along a circle (1.5 mm in diameter) around the centre of the fovea (macular area) for the same subject is depicted. Higher values correspond to the areas where corneal and retinal contributions add together (parallel axes). These areas are the brighter arms of the bow-tie pattern mentioned above.

The bow-tie shape of the ocular retardation distribution in the macular area allows an easy computation of the corneal retardation by means of

$$\delta_{\mathrm{cor}} = \frac{\delta_{\max} + \delta_{\min}}{2} \tag{3}$$

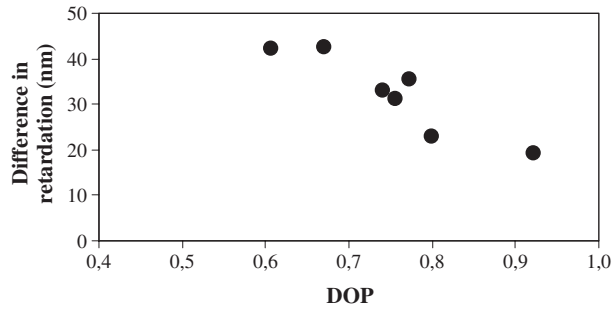

Figure 5. The error in the ocular retardation as a function of the DOP.

with δ_{max} and δ_{min} the maximum and minimum values of the ocular retardation. For this subject the retardation for the cornea was 70 nm (in DP). As expected, this indicates that most of the ocular retardation at that area is due to the cornea (75 nm for the whole eye at the central fovea). In addition, the plot shows that the slow axis lies at 35° ND, close to 40° ND calculated before.

The plot in figure 4 also includes the fit to the retardation function (triangles) result from modelling the eye as a fixed linear retardation for the cornea (70 nm and 35° ND for DP retardation and the slow axis respectively) and a radial retarder (45 nm of DP retardation) for the fovea (please see details in section 3.3).

3.2. The influence of depolarization on ocular polarization parameters

As equations (2) show, the DOP of a light beam is required for the correct determination of polarization parameters associated with ocular birefringence. Table 1 shows the DOP values for the five subjects included in our study. We have also included the results for two additional older eyes (aged 67 and 70). Older eyes present a lower DOP than young adult eyes (greater depolarization effects).

To check the influence of depolarization effects on the determination of the retardation using DP images, we proceeded as follows. The retardation obtained using equations (2) but assuming that the light emerging from the eye is totally polarized, $\delta_{DOP=1}$, was computed. Afterwards, $\delta_{DOP=1}$ was compared to the real retardation (δ_{real}) shown in figure 3.

Figure 5 shows individual DOP values together with the difference between $\delta_{DOP=1}$ and δ_{real} in absolute value. For the set of subjects studied here the error in retardation increases when the DOP reduces. This indicates that in older eyes the accuracy in calculating the ocular retardation is smaller than in young eyes when the actual value of the DOP is not taken into account.

3.3. The influence of corneal birefringence on ocular polarization parameters

The light emerging from the eye provides information on all the ocular structures. In this sense, as described in the introduction, the extraction of retinal information requires the correct subtraction of the corneal contribution.

Table 1. DOP values and ages of the subjects involved in the present study.

Subject	Age	DOP
1	24	0.92
2	27	0.76
3	30	0.80
4	32	0.77
5	41	0.74
6	67	0.61
7	70	0.67

Figures 6(a) and (c) show the macular retardation maps recorded with a commercial polarimeter with a fixed corneal compensator in the two eyes of the same young adult subject. As expected, the fixed corneal compensator does not cancel the corneal birefringence in the two eyes. Compensation for the right eye is fairly good (the presence of a weak bow-tie reveals some residual retardation). For the left eye the corneal compensation is far from the correct one, and the measured total retardation has increased instead of being reduced.

The distributions of the retardation (or alternatively, the retinal nerve fibre layer (RNFL) thickness) around the papilla are also presented in figures 6(b) and (d). The right eye (figure 6(b)) shows a normal retardation pattern: the superior and the inferior nerve fibre bundles are thicker than the nasal and the temporal ones. However, the papilla of the left eye (figure 6(d)) presents a supernormal retardation pattern result from the non-compensation provided by the fixed corneal compensator. Moreover, the double-hump pattern is rotated.

In contrast, when using a commercial system which incorporates an individualized anterior segment compensator, the compensation is accurate and the retardation map of the papillary region becomes normal (figure 7).

We are interested in checking the influence of the corneal compensation on the macular retardation and axis maps. With this goal we have simulated a polarization-based eye model. A DP set 'corneal compensator + right eye' has been modelled using the Mueller matrix formalism. This model does not include effects of depolarization. The corneal compensator consisted of a single retardation plate with a retardation of 60 nm and a fast axis oriented at 15° ND. For the cornea we used another fixed linear retarder with retardation δ_{cor} and fast axis α_{cor}. Since we modelled a right eye, the corneal slow axis (90° apart from the fast one) was supposed to be along the ND direction. Finally, the retina (macula) is described by a uniform retarder ($\delta_{ret} = 22$ nm) with its axis, γ, radially oriented. The Mueller matrix of the whole eye for the macular area for DP is given by (see [38–40] for further information on this model)

$$M_{eye}^{DP}(\gamma) = M_{cc}M_{cor}M_{ret}(\gamma)M_{ret}(\gamma)M_{cor}M_{cc} \qquad (4)$$

where M_{cc}, M_{cor} and $M_{ret}(\gamma)$ are the Mueller matrices of the corneal compensator, the cornea and the macula respectively. Angle γ is measured from the horizontal nasal meridian (negative in the clockwise direction). The values of the retardation and axis were chosen within ranges previously published.

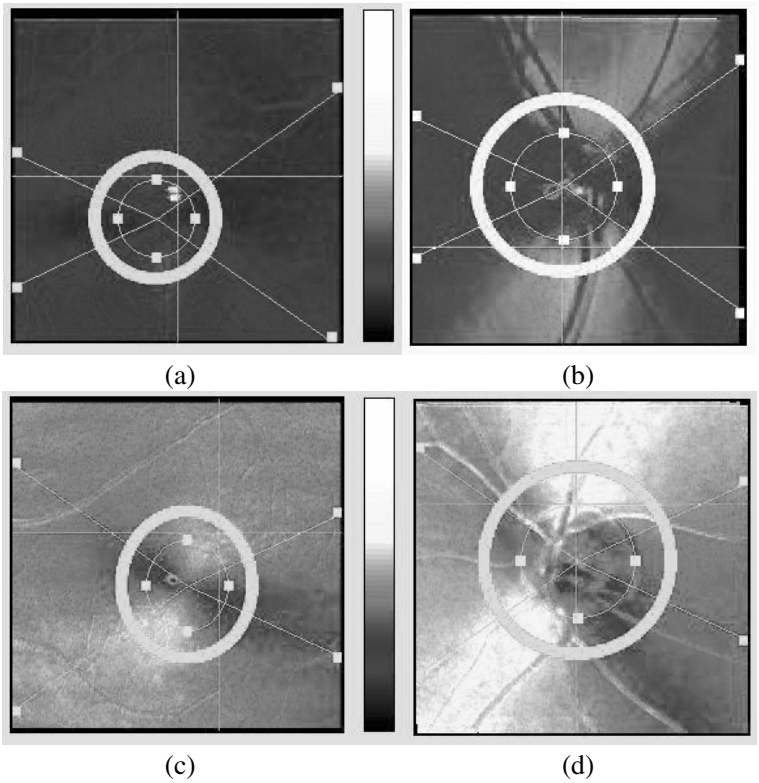

Figure 6. Macular (left) and peripapillary (right) retardation maps for the two eyes of the same subject (right eye, upper panels; left eye, bottom panels) recorded with a commercial scanning laser polarimeter including a fixed corneal compensator.

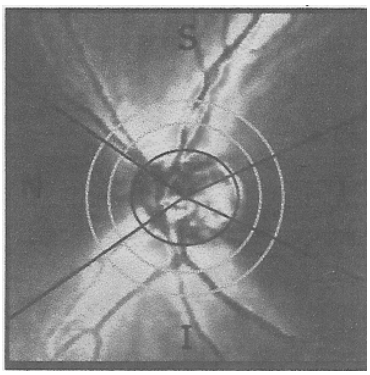

Figure 7. Distribution of the retardation around the papilla of the left eye of the same subject as in the previous figure. The image was registered using a commercial polarimeter including an individual corneal compensator.

For each angle γ, the Mueller matrix of the eye for DP was calculated and the retardation, the axis and the ellipticity of the equivalent retarder were computed by using the theorem reported by Gil and Bernabeu for non-depolarizing optical systems [41]. Since for all simulations the total ocular ellipticity was null, this parameter will not be shown in the following.

In figure 8(a) we show the results for this eye model calculated along a perifoveal annulus (like the thicker one inserted in figure 6) for different experimental situations. Black circles represent the DP ocular retardation when the corneal compensator was not included (just the cornea and retina for DP, $\delta_{\mathrm{cor}} = 60$ nm, $\alpha_{\mathrm{cor}} = 75°$ and $\delta_{\mathrm{ret}} = 22$ nm). Along this circle, retardation arising from these two linear retarders is added or subtracted depending on the relative angle between their axes. The values agree with the typical bow-tie pattern around the centre of the fovea, with troughs 180° apart and peaks 180° apart. The highest values are associated with areas where corneal and retinal axes are aligned. In contrast, the lowest values are a result of areas where corneal and retinal axes are perpendicular. For this particular case, the ocular retardations are 164 nm ($2 \times 60 + 2 \times 22$) and 76 nm ($2 \times 60 - 2 \times 22$). As expected, the DP corneal retardation calculated from equation (3) gives 120 nm (2×60). Furthermore, the slow axis of the cornea can also be calculated from the location of the minimum retardation: $-15°$ (15 ND) for this case, which agrees with the nominal value of the simulated cornea.

Dashed lines correspond to the retardation for a DP through the retina ($2 \times 22 = 44$ nm), that is, when the corneal compensator totally neutralizes the corneal birefringence (retardation and axis).

Triangles in figure 8(a) correspond to a compensation for the corneal axis ($\alpha_{\mathrm{cor}} = 75°$) but not for the retardation ($\delta_{\mathrm{cor}} = 87$ nm $\neq 60$ nm). Due to this undercompensation, the retardation now ranges from 10 to 98 nm and the modulation increases from 0.37 to 0.81. However, the orientation of the corneal axis can still be correctly extracted from these data. On the other hand, if the corneal retardation is well compensated ($\delta_{\mathrm{cor}} = 60$ nm) but the fast axes for the cornea and the compensator are not 90° apart ($\alpha_{\mathrm{cor}} = 55°$ nm $\neq -15° + 90°$), the resulting retardation pattern differs from the previous one (squares in figure 8(a)). Although the amplitude also remains

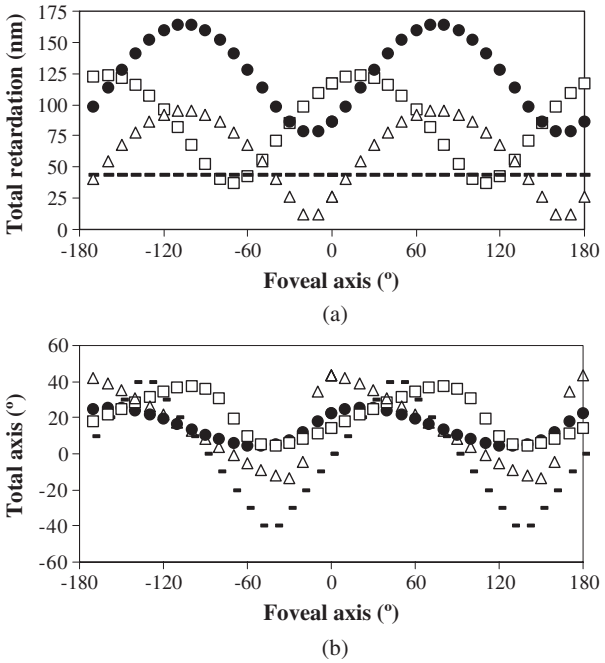

Figure 8. The total DP retardation (a) and axis (b) along an annulus around the fovea in a simulated set 'corneal compensator + right eye' for different situations: without a compensator (circles, mean = 124 nm), total corneal compensation (dashes), compensation of corneal retardation (squares, mean = 87 nm) and compensation of corneal axis (triangles, mean = 60 nm).

constant, the modulation decreases to 0.54. For this situation the slow axis moves towards larger ND orientations ($-70°$).

Values of the total ocular axis are plotted in figure 8(b). Black circles correspond to the axis of the complete eye. This is also a function of the period π, whose values range from 4° to 26°. When the cornea is totally compensated, the axis corresponds to the radial distribution of the fovea (dashes). However, this distribution changes noticeably for the other two situations described above. For these cases, at each point of the annulus around the fovea centre the resultant axis depends on the combination of the axes of three retarders involved: two fixed (the cornea and the compensator) and one with a radial distribution (the retina).

To complete this study, figure 9 reports on two additional cases of a non-compensated cornea: undercompensation ($\delta_{cor} = 87$ nm > 60 nm) represented by black diamonds and overcompensation ($\delta_{cor} = 33$ nm < 60 nm) represented by black triangles. For both situations the corneal axis is not neutralized ($\alpha_{cor} = 55° \neq -15° + 90°$). In order to compare these results, the data for a total corneal retardation compensation are also plotted (white symbols). Since the axes are identical for the three situations, the shapes of the three retardation signals are similar despite some horizontal (in foveal axis) and vertical (in total retardation) displacements. In addition, amplitudes are maintained but the modulations are different (0.40 and 0.47 for undercompensation and overcompensation respectively) because of changes in maximum and minimum retardations. For this particular case, the maximum value corresponds to the undercompensation case (151 nm) and is located at 30°, a value which differs from the corneal fast axis (55°).

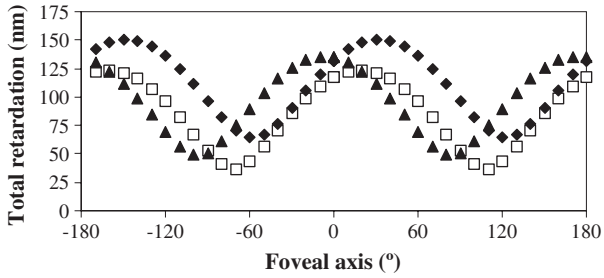

Figure 9. The total retardation for the same polarization eye model as in the previous figure when the corneal compensator undercompensates (black diamonds, mean = 112 nm) and overcompensates (black triangles, mean = 98 nm) the corneal retardation. In both cases, the corneal axis is not compensated either. The white squares are the same as in figure 8(a).

4. Discussion

It has been reported that ocular diattenuation is low [4, 8, 10, 38, 42], which indicates that, as a first approximation, the eye can be considered as a birefringent medium with some depolarizing effects. In addition, this birefringence is linear [4, 15–18] and δ, α and the DOP can be computed from the Stokes vector of the light emerging from the eye. In the present experimental set-up the incident beam is perpendicular to the centre of the cornea and focuses on a single point at the central fovea (∼5 arcmin). This area is free of nerve fibres and shows just a small birefringence due to the Henle fibre layer. Since the associated retardation is much smaller than that due to the cornea [14, 17], we can assume that the cornea is the main factor in the retardation computed using DP images.

The ND distribution of the central corneal axis depicted in figure 3 agrees with those from previous experiments [9, 11, 15, 16, 19] using different techniques. In particular, Knighton and Huang [11] used a corneal polarimeter which provided a view of the fourth Purkinje image to study the corneal birefringence in a sample of 73 subjects. They reported that the peak of the axis distribution falls between 10° and 20° ND, with values ranging from 13° nasally upward to 72° ND. Our data also fall within this range.

The values of retardation depend on the subject; however, the range is also similar to those reported by other authors [9, 11, 15–22]. Previous literature [11] stated that eyes with weaker retardations were associated with more ND axes. Since few subjects were involved in this experiment, this cannot be corroborated.

On the other hand, we found that depolarization effects are larger in older eyes in the set of subjects studied here (table 1). Results for young eyes agree with those from previous *in vivo* experiments [16, 18, 31, 34]. Data on depolarization in older eyes have not been found in the literature.

The most important source of depolarization in normal young eyes is the retina [33, 34, 43]. Although the depolarization effects in healthy young eyes are slight, they may increase with age, in part due to the loss of transparency of the ocular media [44, 45]. Age-related pathologies are also a source of retinal depolarization [26]. In young eyes, corneal refractive surgery could also increase depolarization effects [28, 46].

Moreover, depolarization is important when calculating the parameters of polarization, in particular the retardation, as figure 5 shows. We have calculated the retardation supposing DOP = 1 ($\delta_{\mathrm{DOP=1}}$). This parameter has been compared to the actual retardation (δ_{real}) calculated using equations (2) also but including the real value of the DOP. On average, the lower the DOP, the higher the error in the retardation calculated. In view of this, since the error in the measured retardation increases when the DOP decreases, it is convenient to include the actual effects of depolarization when calculating the ocular retardation, especially in the analysis of subjects who are prone to having larger levels of ocular depolarization.

In a previous work, this author compared the ocular parameters of polarization calculated using a complete Mueller matrix polarimeter and a linear polariscope [35]. The results were similar due to the low depolarization levels. Burns and colleagues have used the depolarized light emerging from the eye to enhance the contrast of subretinal changes in age-related maculopathy [27].

Referring to the ocular retardation measured around a fovea-centred annulus in the macula (perifoveal retina) (figure 4), this is found to be a combined effect of the birefringence of the cornea and the radially arranged Henle fibres. This agrees with the following features:

(1) the central cornea acts as a fixed linear retarder with the slow axis along the ND direction;
(2) the perifoveal retardation is uniform along a circle around the fovea; and
(3) the distribution of the foveal slow axis is radial.

A system composed of any number of retarders (linear, circular or elliptical) is optically equivalent to a linear retarder plus a rotator [47]. The combination of these two elements requires a polar decomposition theorem such as that described in [41] or [36] to extract the equivalent parameters of polarization.

Black circles in figure 8(a) correspond to this combination in the eye. This pattern of retardation corresponds to a bow-tie and presents a π-periodic behaviour. Because the retinal retardation is uniform along a perifoveal annulus and the axis distribution is radially symmetrical, any modulation of the measured retardation in that area must result from uncompensated, or erroneously compensated, retardation elsewhere in the light pathway. Commercial scanning laser polarimeters oriented to glaucoma diagnosis incorporate a fixed corneal compensator intended to neutralize the corneal birefringence. The corneal component of the retardation will be cancelled if the corneal slow axis is parallel to the compensator fast axis and the two magnitudes of the birefringence are equal (dashed line in figure 8(a)). In a spatially resolved distribution of retardation, a total corneal cancellation provides a uniform map of retinal retardation [18, 22].

In this sense, if the corneal and compensator fast axes are 90° apart but the corneal retardation is undercompensated, the computed retardation does not correspond to the retinal one, but will be the result of the combination of the compensator, the cornea and the retina. For this situation both minimum and maximum retardation values decrease and modulation increases, but their location and the amplitude of the signal remain constant. Now equation (3) will give a wrong retardation for the cornea; however, the orientation of the corneal axis can be correctly computed from the distribution of the perifoveal retardation.

If corneal retardation is reached but fast axes are not perpendicular, the ocular retardation pattern differs from that obtained in the above case, although the amplitude of the signal also remains constant. The most important change is that the retardation pattern moves and the corneal axis cannot be determined by locating the minimum retardation any longer. In a spatial resolution this is represented by a rotation of the bow-tie pattern. As a direct consequence, the papillary retardation map is also rotated, showing erroneous values (see figure 6(b)).

Results on the ocular axis also show a periodic distribution around the fovea centre (see figure 8(b)). The amplitude of the signal increases noticeably when considering a total corneal compensation and the resultant ocular axis is just the radial distribution of the retinal axis itself. When considering the corneal compensations in the retardation and axis separately, the signal remains periodic but its shape changes and its symmetry around the maximum (and the minimum) disappears.

When neither the corneal retardation nor the corneal axis are compensated, the amplitudes of the ocular retardation around the fovea are maintained with respect to the signal obtained when there is just retardation compensation (figure 9). However, the modulations change depending on the difference between the corneal and compensator retardations. Moreover, the locations of the maximum and minimum values are displaced, which indicates a rotation in the arms of the macular bow-tie.

A real situation with a lack of corneal compensation can be found in figure 6(c). As a direct consequence of this, the global retardation is overestimated instead of being cancelled. This macular retardation seems to be much higher than that corresponding to the right eye of the same subject.

The effects of using a fixed corneal compensator have been a topic of study for several authors in the last few years. Most of the time these works have reported an influence of an erroneous corneal compensation on the estimation of the RNFL thickness, the basis of glaucoma diagnosis. This paper is not centred on this topic, but on exploring the effects of a lack of corneal compensation on the retardation and axis distribution around the macular area.

Greenfield *et al* [19] first reported, for 112 eyes of 63 subjects, that there is considerable inter-individual variation in the corneal axis. They demonstrated that the corneal axis is significantly associated with RNFL and macular polarization parameters. The effects of the individual corneal compensation on the determination of the spatially resolved RNFL thickness have been studied in [22].

Because the axons of the RNFL are approximately radially arranged in the peripapillary retina, the interaction of the set 'corneal compensator plus cornea' with the peripapillary RNFL birefringence may be similar to that occurring in the macula described above. This can be observed in figure 6(d). In this papillary retardation map the areas with higher retardation (thicker RNFL) are aligned with the brighter arms of the macular map of figure 6(c), instead of being along the vertical meridian as shown in figure 6(b). Furthermore, not only are the thicker RNFL areas rotated

with respect to those of a normal eye, but also the thickness is overestimated, which may cause underestimation of the presence of glaucomatous signals. On the other hand, when the correct corneal compensation is used (figure 7), the pattern of peripapillary retardation is normal.

Garway-Heath and colleagues [20] proposed using the macular retardation pattern to correct peripapillary measurements for erroneously compensated corneal birefringence. Looking at the relationship between the retardation in the two areas and between the peripapillary retardation and the visual field mean deviation, they were able to improve the discrimination between normal and glaucomatous eyes. They found a strong correlation between the perifoveal and the peripapillary retardations, suggesting that a substantial part of the retardation measured in the peripapillary region arises from the interaction of the cornea and the corneal compensator.

Knighton and co-workers [40] have reported an extensive analytical model for explaining the role of the corneal compensator in scanning laser polarimetry. They simulated eyes with different corneal and retinal retardations and reported the results for the modulation, mean and bow-tie axis, without using a decomposition theorem to extract the retardation as in our case. They just used a very simple expression and did not take into account other polarization parameters related to birefringence such as the axis and ellipticity. Reported measurements on a large number of living human eyes showed that the slow axis of the set formed by the corneal compensator and the cornea is approximately vertical. The bow-tie axis of the macular region usually exaggerated the anatomic double-hump pattern of the RNFL, as also shown here.

In conclusion, the work presented here has shown that although the corneal retardation and slow axis are particular to each subject, the latter lies along the ND direction. The erroneous cancellation of every particular corneal birefringence produces non-uniform macular retardation maps which lead to a wrong estimation of the corneal and retinal polarization parameters. Since the present paper is not centred on glaucoma diagnosis, the effect of the corneal birefringence on the ocular retardation has been studied from a more basic point of view, including effects on the axis distribution which commercial polarimeters do not measure. Moreover, the influence of depolarization effects on the measured ocular retardation have also been analysed. The lower the DOP, the larger the error in the retardation. This could be very important for older eyes, which present lower DOP values. In addition, older eyes require more accurate retardation measurement because they tend to suffer from retinal pathologies including glaucoma, that could be additional sources of depolarization.

Acknowledgments

The author thanks E Berrio for her valuable assistance during the development of the imaging polarimeter and the data collection, and Professor P Artal for helpful ideas and providing the optical elements used in the experimental system. D F Garway-Heath and R Foster are also gratefully acknowledged for providing the GDx images.

References

[1] Bour L J 1991 Polarized light and the eye *Vision Optics and Instrumentation* vol 1, ed W N Charman (London: Macmillan) chapter 13

[2] Born M and Wolf E 1999 *Principles of Optics* 7th edn (New York: Pergamon)

[3] Dreher A W and Reiter K 1992 Scanning laser polarimetry of the retinal nerve fiber layer *Proc. SPIE* **1746** 36–41

[4] Dreher A W, Reiter K and Weinreb R N 1992 Spatially resolved birefringence of the retinal never fiber layer assessed with a retinal laser ellipsometer *Appl. Opt.* **31** 3730–5

[5] Weinred R N, Dreher A W, Coleman A, Quigley H, Shaw B and Reiter K 1990 Histopathologic validation of Fourier-ellipsometry measurements of retinal nerve-fiber layer thickness *Arch. Ophthalmol.* **108** 557–60

[6] Weale R A 1978 On the birefringence of the human crystalline lens *J. Physiol.* **284** 112–3

[7] Klein Brink H B 1991 Birefringence of the human crystalline lens *in vivo J. Opt. Soc. Am.* A **8** 1788–93

[8] Bueno J M and Campbell M C W 2003 Polarization properties for *in vitro* old human crystalline lens *Ophthalm. Physiol. Opt.* **23** 109–18

[9] van Blokland G J and Verhelst S C 1987 Corneal polarization in the living human eye explained with a biaxial model *J. Opt. Soc. Am.* A **4** 82–90

[10] Bueno J M and Jaronski J W 2001 Spatially resolved polarization properties for *in vitro* corneas *Ophthalm. Physiol. Opt.* **21** 384–92

[11] Knighton R W and Huang X-R 2002 Linear birefringence of the central human cornea *Invest. Ophthalmol. Vis. Sci.* **43** 82–6

[12] Bueno J M and Vargas-Martín F 2002 Measurements of the corneal birefringence with a liquid-crystal imaging polariscope *Appl. Opt.* **41** 116–24

[13] Jaronski J W and Kasprzak H T 2003 Linear birefringence measurements of the *in vitro* human *Ophthalm. Physiol. Opt.* **23** 361–9

[14] Klein Brink H B and van Blokland G J 1988 Birefringence of the human foveal area assessed *in vivo* with Mueller-matrix ellipsometry *J. Opt. Soc. Am.* A **5** 49–57

[15] Bueno J M 2000 Measurement of parameters of polarization in the living human eye using imaging polarimetry *Vis. Res.* **40** 3791–9

[16] van Blokland G J 1985 Ellipsometry of the human retina *in vivo*: preservation of polarization *J. Opt. Soc. Am.* A **2** 72–5

[17] Pelz B, Weschenmoser C, Goelz S, Fischer J P, Burk R O W and Bille J F 1996 *In vivo* measurement of the retinal birefringence with regard on corneal effects using an electro-optical ellipsometer *Proc. SPIE* **2930** 92–101

[18] Pelz B C E 1997 Entwicklung eines elektrooptischen ellipsometers zur *in vivo* evaluation der retinalen nervenfaserschicht und der hornhaut des menschlichen auges *PhD Thesis* Universität Heidelberg

[19] Greenfield D S, Knighton R W and Huang X-R 2000 Effect of corneal polarization axis on assessment of retinal nerve fiber layer thickness by scanning laser polarimetry *Am. J. Ophthalmol.* **129** 715–22

[20] Garway-Heath D F, Greaney M J and Caprioli J 2002 Correction for the erroneous compensation of anterior segment birefringence with the scanning laser polarimeter for glaucoma diagnosis *Invest. Ophthalmol. Vis. Sci.* **43** 1465–74

[21] Greenfield D S, Knighton R W, Feuer W J, Schiffman J C, Zangwill L and Weinreb R N 2002 Correction for corneal polarization axis improves the discriminating power of scanning laser polarimetry *Am. J. Ophthalmol.* **134** 27–33

[22] Zhou Q and Weinreb R N 2002 Individualized compensation of anterior segment birefringence during scanning laser polarimetry *Invest. Ophthalmol. Vis. Sci.* **43** 2221–8

[23] Weinreb R N, Bowd C and Zangwill L 2002 Scanning laser polarimetry in monkey eyes using variable corneal polarization compensation *J. Glaucoma* **11** 378–84
[24] Medeiros F A, Zangwill L M, Bowd C, Bernd A S and Weinred R N 2003 Fourier analysis of scanning laser polarimetry measurements with variable corneal compensation in glaucoma *Invest. Ophthalmol. Vis. Sci.* **44** 2606–12
[25] Bagga H, Greenfield D S and Knighton R W 2003 Scanning laser polarimetry with variable corneal compensation: identification and correction for corneal birefringence in eyes with macular disease *Invest. Ophthalmol. Vis. Sci.* **44** 1969–76
[26] Burns S A, Elsner A E, Mellem-Kairala M B and Simmons R B 2003 Improved contrast of subretinal structures using polarization analysis *Invest. Ophthalmol. Vis. Sci.* **44** 4061–8
[27] Bueno J M, Berrio E, Marín J M and Artal P 2002 Polarization and aberrations in normal and post-LASIK eyes assessed with an aberro-polariscope *Annual Mtg Abstract and Program Planner* (Rockville, MD: Association for the Research in Vision and Ophthalmology) accessed at http://www.arvo.org (Abstract 2048)
[28] Berrio E, Bueno J M, Redondo M and Artal P 2003 Does intraocular scattering increase after LASIK refractive surgery? *Annual Mtg Abstract and Program Planner* (Rockville, MD: Association for the Research in Vision and Ophthalmology) accessed at http://www.arvo.org (Abstract 2136)
[29] Angeles R, Abunto T, Schanzlin D, Zangwill L M, Bowd C and Weinreb R N 2003 Corneal changes after laser *in situ* keratomileusis: measurement of corneal polarization and magnitude *Annual Mtg Abstract and Program Planner* (Rockville, MD: Association for the Research in Vision and Ophthalmology) accessed at http://www.arvo.org (Abstract 2666)
[30] Abunto T, Angeles R, Zangwill L M, Bowd C, Schanzlin D and Weinreb R N 2003 Retinal nerve fiber layer thickness measurements after laser assisted *in situ* keratomileusis (LASIK) *Annual Mtg Abstract and Program Planner* (Rockville, MD: Association for the Research in Vision and Ophthalmology) accessed at http://www.arvo.org (Abstract 3399)
[31] Bueno J M and Artal P 1999 Double-pass imaging polarimetry in the human eye *Opt. Lett.* **24** 64–6
[32] Bueno J M, Berrio E and Artal P 2003 Aberro-polariscope for the human eye *Opt. Lett.* **28** 1209–11
[33] van Blokland G J and van Norren D 1986 Intensity and polarization of light scattered at small angles from the human fovea *Vis. Res.* **26** 485–94
[34] Bueno J M 2001 Depolarization effects in the human eye *Vis. Res.* **41** 2687–96
[35] Bueno J M 2002 Polarimetry in the human eye using an imaging linear polariscope *J. Opt. A: Pure Appl. Opt.* **4** 553–61
[36] Lu S and Chipman R A 1996 Interpretation of Mueller matrices based on polar decomposition *J. Opt. Soc. Am.* A **13** 1106–13
[37] Bueno J M and Campbell M C W 2002 Confocal scanning laser ophthalmoscopy improvement by use of Mueller-matrix polarimetry *Opt. Lett.* **27** 830–2
[38] Bueno J M 1999 Estudio de las propiedades de polarización del ojo humano *PhD Thesis* Universidad de Murcia
[39] Hunter D G, Sandruck J C, Sau S, Patel S N and Guyton D L 1999 Mathematical modeling of retinal birefringence scanning *J. Opt. Soc. Am.* A **12** 2103–11
[40] Knighton R W, Huang X-R and Greenfield D S 2002 Analytical model of scanning laser polarimetry for retinal nerve fiber layer assessment *Invest. Ophthalmol. Vis. Sci.* **42** 383–92
[41] Gil J J and Bernabeu E 1987 Obtainment of the polarizing and retardation parameters of a non-depolarizing optical system from the polar decomposition of its Mueller matrix *Optik* **76** 67–71
[42] Bone R A 1980 The role of the macular pigment in the detection of polarized light *Vis. Res.* **20** 213–9
[43] Burns S A, Wu S, Delori F C and Elsner A E 1995 Direct measurement of human-cone-photoreceptor alignment *J. Opt. Soc. Am.* A **12** 2329–38
[44] Ijspeert J K, de Waard P W, van der Berg T J and de Jong P T 1990 The intraocular stray-light function in 129 healthy volunteers; dependence on angle, age and pigmentation *Vis. Res.* **30** 699–707
[45] Hennelly M L, Barbur J L, Edgar D F and Woodward E G 1998 The effect of age on the light scattering characteristics of the eye *Optom. Vis. Sci.* **18** 197–203
[46] Lohmann C P, Fitzke F, O'Brart D, Muir K M and Marshall J 1993 Corneal light scattering and visual performance in myopic individuals with spectacles, contact lenses, or excimer laser keratectomy *Am. J. Ophthalmol.* **115** 444–53
[47] Hurwitz H and Jones R C 1941 A new calculus for the treatment of optical systems: II. Proof of three general equivalence theorems *J. Opt. Soc. Am.* **31** 493–9